CMS Physics Analysis Summary

Contact: cms-pag-conveners-susy@cern.ch 2017/07/06

Search for supersymmetry in events with at least one soft lepton, low jet multiplicity, and missing transverse momentum in proton-proton collisions at $\sqrt{s} = 13$ TeV

The CMS Collaboration

Abstract

A search for supersymmetry with a compressed mass spectrum using events with a high-momentum jet attributed to initial state radiation, high missing transverse momentum, and a low-momentum lepton is presented. In particular, scenarios of top squark pair production are investigated, where the mass difference to the lightest supersymmetric particle (LSP) is smaller than the mass of the W boson. The search is performed in a sample of proton-proton collisions recorded with the CMS detector at a centre-of-mass energy of 13 TeV corresponding to an integrated luminosity of 35.9 fb^{-1}. The results are consistent with the expectation from standard model processes and limits are set on the production cross section in the plane of the top squark vs. LSP masses. The signal models used for the interpretation of the results assume either four-body decays of the top squark, $\widetilde{t} \to \mathrm{b}ff'\mathrm{LSP}$, or decays via an intermediate chargino, $\widetilde{t} \to \mathrm{b}\widetilde{\chi}_1^+ \to \mathrm{b}ff'\mathrm{LSP}$. Assuming a 100% branching ratio of the corresponding decay, top squark masses below 500 (540) GeV for four-body (chargino-mediated) decay are excluded at 95% confidence level for a mass difference to the LSP of about 30 GeV. These limits are currently the most stringent in the single lepton final state and are similar to those of analyses targeting other final states in this region of supersymmetry parameter space with 2016 data.

1 Introduction

The main objectives of the CERN LHC programme include searches for new physics. Supersymmetry (SUSY) [1–5] is one of the most promising extensions of the standard model (SM) of particle physics. Supersymmetric models can offer solutions to several shortcomings of the SM, in particular those related to the mass hierarchy of elementary particles [6, 7] and to the presence of dark matter in the universe.

Supersymmetry predicts superpartners of SM particles (sparticles) whose spins differ by one-half unit with respect to their SM partners. In SUSY models with R-parity [8] conservation, sparticles are pair-produced and their decay chains end with the lightest supersymmetric particle (LSP). In many of these models the lightest neutralino ($\widetilde{\chi}_1^0$) takes the role of the LSP and, being neutral and weakly interacting, would match the characteristics required of a dark matter candidate. The LSPs would remain undetected and yield a characteristic signature of high missing transverse momentum $p_{\mathrm{T}}^{\mathrm{miss}}$.

There are a number of scenarios in which sparticle production at the LHC could evade existing searches. We investigate scenarios in which the mass splitting between the next-to-lightest SUSY particle and the LSP is small, which is referred to as "compressed SUSY". In this case, the SUSY signal would escape classical search strategies because of the low transverse momenta (p_{T}) of the decay products. Signal events can still be distinguished from SM processes if a high-p_{T} jet from initial-state radiation (ISR) leads to a boost of the sparticle pair system and enhances the amount of $p_{\mathrm{T}}^{\mathrm{miss}}$, while the other decay products typically remain soft. In the signal scenarios studied in this paper, SUSY particles can decay leptonically, and the presence of low-p_{T} leptons can be used to discriminate further against otherwise dominant SM backgrounds, such as multijet production and Z+jets events with Z boson decays to neutrinos.

SUSY models with light top squarks ($\widetilde{\mathrm{t}}$) are well motivated as they control the dominant correction to the Higgs boson mass and thereby preserve "naturalness" [6, 7, 9–14]. SUSY scenarios with mass splittings of 15–30 GeV between the top squark and the LSP are especially interesting because they would lead, through $\widetilde{\mathrm{t}}$-$\widetilde{\chi}_1^0$ co-annihilation, to the observed cosmological abundance of dark matter [15]. For mass differences below the W-boson mass, top squarks could undergo either a two-body decay ($\widetilde{\mathrm{t}} \to \mathrm{c}\widetilde{\chi}_1^0$) or a four-body decay ($\widetilde{\mathrm{t}} \to \mathrm{bff}'\widetilde{\chi}_1^0$, where ff′ represents a pair of quarks or leptons from a virtual W boson), as shown in Fig. 1(left), with branching fractions that depend on details of the model. Alternatively, the decay $\widetilde{\mathrm{t}} \to \mathrm{b}\widetilde{\chi}^+ \to \mathrm{bff}'\widetilde{\chi}_1^0$ shown in Fig. 1(right) is possible if the mass of the lighest chargino is lower than the top squark mass.

In this document we describe a search for pair production of top squarks in events with a high-p_{T} jet, $p_{\mathrm{T}}^{\mathrm{miss}}$, and at least one soft lepton, corresponding to signal events with a leptonic decay of at least one of the virtual W bosons. The single-lepton topology offers the second-highest branching fraction after the purely hadronic mode. In this channel we consider muons and electrons, which can be efficiently reconstructed and identified with transverse momenta as low as 5 GeV. In addition, selected events are required to have a hard jet compatible with the ISR signature, at most one additional jet of moderate to high p_{T}, no hard leptons, and a significant amount of $p_{\mathrm{T}}^{\mathrm{miss}}$. The dominant remaining SM backgrounds to this search are pair production of top quarks and W boson production in association with jets. Their contributions to signal regions are estimated by correcting the predictions from simulation using the event yields observed in several control regions in data. Data are also used to validate this procedure and to derive systematic uncertainties. The results are interpreted in two signal scenarios, assuming a 100% branching ratio either for the four-body decay or the chargino-mediated decay.

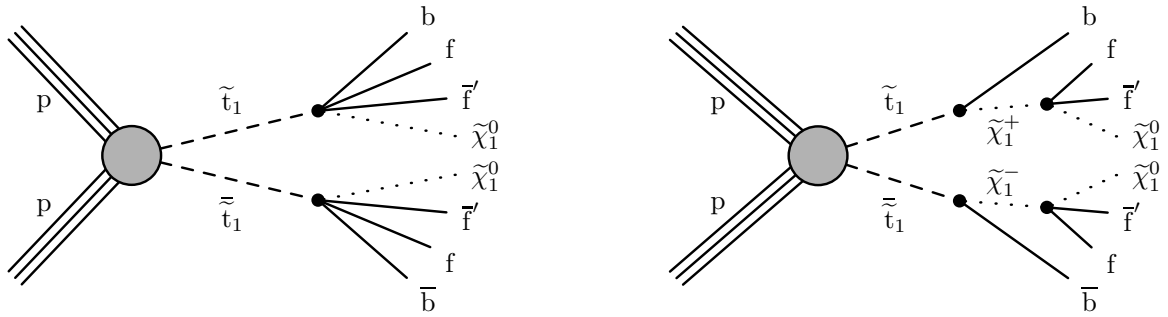

Figure 1: Signal models for top squark pair production with subsequent four-body (left) or chargino-mediated (right) decays.

The most recent result from CMS targeting the four-body decay in the single lepton final state is [16] while the interpretation using the chargino-mediated decay is presented here for the first time. The most recent ATLAS result studying similar SUSY parameter space in the single lepton final state is [17]. Similar results were obtained also in all-hadronic final state [18] and di-lepton final state [19].

2 Detector and object definition

The CMS detector has been described in detail in Ref. [20]. Its central feature is a superconducting solenoid that provides a homogeneous field of 3.8 T in a volume containing a silicon pixel and strip tracker, a lead tungstate crystal electromagnetic calorimeter, and a brass and scintillator hadron calorimeter. Muons are measured in gas-ionization chambers embedded in the steel flux-return yoke surrounding the solenoid. The acceptance of the silicon tracker and the muon systems extends to pseudorapidities of $|\eta| < 2.5$ and < 2.4, respectively. The barrel and endcap calorimeters cover the range $|\eta| < 3.0$ and are complemented by extensive forward calorimetry. Events are selected for further analysis by a two-tier trigger system that uses custom hardware processors to make a fast initial selection, followed by a more detailed selection executed on a dedicated processor farm.

The measurement of jets and $p_{\mathrm{T}}^{\mathrm{miss}}$ is based on candidates reconstructed by the particle-flow (PF) algorithm [21], which identifies leptons, photons, and charged and neutral hadrons by combining information from all subdetectors. The PF candidates are clustered into jets by using the anti-k_{T} algorithm [22] with a distance parameter of 0.4. Jets are required to have $p_{\mathrm{T}} > 30\,\mathrm{GeV}$ and $|\eta| < 2.4$, and to pass loose quality criteria [23] based on the energy fractions associated with electromagnetically or hadronically interacting charged or neutral particles. The negative vector sum of the transverse momenta of the PF candidates defines the value of $p_{\mathrm{T}}^{\mathrm{miss}}$ and the corresponding direction. Jet energies and $p_{\mathrm{T}}^{\mathrm{miss}}$ are corrected for shifts in the energy scale, contributions from additional, simultaneous proton-proton collisions (pileup), and residual differences between data and simulation [24, 25]. Jets originating from b quarks are identified ("tagged") using the combined secondary vertex algorithm [26, 27] at a working point corresponding to an efficiency of about 70% and a misidentification probability for light-quark jets of about 1%. Hadronic decays of τ leptons are identified using the "hadrons-plus-strips" algorithm [28, 29].

Muons and electrons are required to have p_{T} above 3.5 GeV and 5 GeV, respectively. Standard loose identification requirements [30, 31] are applied to reduce the background from non-prompt leptons produced in semileptonic hadron decays and from jets misidentified as leptons.

Further background reduction is achieved by requiring the leptons to be isolated. The absolute isolation I_{abs} is computed by summing the transverse momenta of PF candidates, except that of the lepton, in a cone of size $\Delta R < 0.3$ around the lepton direction, where $\Delta R \equiv \sqrt{(\Delta\phi)^2 + (\Delta\eta)^2}$ and ϕ is the azimuthal angle measured in radians. The energy in the isolation cone is corrected for the effects of pileup. The relative isolation I_{rel} is obtained by dividing I_{abs} by the p_{T} of the lepton. The details of the isolation requirements are described in Section 4.

3 Samples and event preselection

The data sample comprises proton-proton collisions recorded in the 2016 run at a centre-of-mass energy of 13 TeV and corresponds to an integrated luminosity of 35.9 fb^{-1}. The search uses events passing one of several online $p_{\text{T}}^{\text{miss}}$ selections. These triggers evolved over the data-taking period and required $p_{\text{T}}^{\text{miss}}$ to pass thresholds between 90 and 120 GeV, where the online $p_{\text{T}}^{\text{miss}}$ is reconstructed using the PF algorithm. Control samples were collected based on a single-muon or a single-electron trigger with a p_{T} threshold of 24 GeV and 27 GeV, respectively.

Simulated Monte Carlo (MC) samples of SM background events are produced by using several generators. The generation of main background samples, in particular W+jets, $\text{t}\bar{\text{t}}$ and Z/γ^* production is performed with the MADGRAPH5_AMC@NLO 2.3.3 [32] generator at leading order (LO) using the LO NNPDF3.0 [33] parton distribution functions (PDF). The production of single top quarks is simulated by using the POWHEGv2.0 [34] program and the associated tW production using POWHEGv1.0 [35] in next-to-leading order (NLO) using the NLO NNPDF3.0 PDF. Simulations of diboson events are done with MADGRAPH5_AMC@NLO 2.3.3 and POWHEGv2.0 at the NLO. The MADGRAPH5_AMC@NLO 2.3.3 generator is also used to simulate the $\text{t}\bar{\text{t}}$-W and $\text{t}\bar{\text{t}}$-Z processes at LO and the $\text{t}\bar{\text{t}}$-γ production at the NLO. All samples are passed to PYTHIA 8.212 [36, 37] with the CUETP8M1 tune for hadronization and showering. The detector response is simulated with the GEANT4 [38] program. Finally, all events are reconstructed with the same algorithms as the ones used for data. Pileup events are included in the simulation and all samples are reweighted to match the luminosity profile in data.

The signal simulation for $\tilde{\text{t}}$ pair production is done on a grid in the $\tilde{\text{t}}$–$\tilde{\chi}_1^0$ mass plane with $m(\tilde{\text{t}})$ ranging from 250–800 GeV in steps of 25 GeV, and $\Delta m \equiv m(\tilde{\text{t}}) - m(\tilde{\chi}_1^0)$ ranging from 10–80 GeV in steps of 10 GeV. The samples with a $\tilde{\chi}^{\pm}$ in the decay chain are generated with the $\tilde{\chi}^{\pm}$ mass halfway between the $\tilde{\chi}_1^0$ and $\tilde{\text{t}}$ masses. The production of top-squark pairs with up to two additional jets is generated with MADGRAPH5 2.3.3 followed by decay, hadronization and showering in PYTHIA 8.212. In the decay only phase space is considered, the Breit-Wigner distribution of the off-shell W boson is taken into account and the $\tilde{\text{t}}$ decay length is set to zero. For the signal samples, the modelling of the detector response is performed with the CMS fast simulation program [39]. Differences in the efficiencies of the lepton selection and the b-jet identification between the fast and the detailed GEANT4 simulation are corrected for.

The effects of residual differences between data and simulation are taken into account in the analysis. The systematic uncertainty related to possible variations in the jet energy scale [24] is evaluated by a coherent change of all jet energies, which is also propagated to $p_{\text{T}}^{\text{miss}}$. The jet energy resolution in simulation is found to be slightly better than in data [24]. To compensate for this effect, the energies of simulated jets are smeared and a corresponding systematic uncertainty is assigned. Simulation is corrected for differences in the reconstruction and identification efficiencies of leptons [30, 31] and b jets [26, 27] with respect to the values measured in data. The corresponding uncertainties are propagated to the final results.

The first step in the event selection is designed to match the online requirements and to serve

as a common basis for the analysis. It is guided by the general characteristics of signal events. The leading jet of each event is considered as an ISR jet candidate and is required to fulfil $p_T > 100\,\text{GeV}$ and $|\eta| < 2.4$. Since jets resulting from $\tilde{t}$ decays are soft, at most one additional jet with $p_T > 60\,\text{GeV}$ is accepted. At least one identified muon (electron) with $p_T > 3.5(5)\,\text{GeV}$ and $|\eta| < 2.4$ (2.5) must be present. Finally, a requirement of $p_T^{\text{miss}} > 200\,\text{GeV}$ and of $H_T > 300\,\text{GeV}$ is imposed, where H_T is the scalar sum of the transverse momenta of all jets. By using a control sample collected with the single-electron trigger, the efficiency of signal triggers is found to be higher than 90% for $p_T^{\text{miss}} > 200\,\text{GeV}$ and higher than 98% for $p_T^{\text{miss}} > 250\,\text{GeV}$. The simulation samples are reweighted based on this measurement to account for trigger inefficiencies.

4 Event selection

The single-lepton topology is selected by requiring a single muon or electron within the acceptance described in the previous sections. To avoid strong variations of the lepton selection efficiency with p_T, a combined isolation criterion, $I_{\text{abs}} < 5\,\text{GeV}$ or $I_{\text{rel}} < 0.2$, is used, equivalent to a transition from an absolute to a relative isolation requirement at $p_T = 25\,\text{GeV}$. The absolute values of the lepton impact parameters with respect to the primary collision vertex in the transverse plane (d_{xy}) and longitudinal direction (d_z) are required to be smaller than 0.02 and 0.1 cm, respectively. The reconstructed vertex with the largest value of summed physics-object p_T^2 is taken to be the primary pp interaction vertex. The physics objects are the objects returned by a jet finding algorithm [22, 40] applied to all charged tracks associated with the vertex, plus the corresponding associated missing transverse momentum. Events are rejected if a τ lepton, or an additional electron or muon with $p_T > 20\,\text{GeV}$ is present. Background from SM dijet and multijet production is suppressed by requiring the azimuthal angle between the momentum vectors of the two leading jets to be smaller than 2.5 rad for all events with a second hard jet of $p_T > 60\,\text{GeV}$. According to simulation, the remaining sample is dominated by W+jets and, to a lesser extent, by $\text{t}\bar{\text{t}}$ production with a single prompt lepton in the final state. Therefore, we use the transverse mass m_T computed from the transverse components of the lepton momentum and the p_T^{miss} vector as a discriminant.

Distributions of the lepton p_T and of m_T at this stage of the selection are presented in Fig. 2. They show a good agreement between the shapes of these distributions in data and simulation. Small differences in the shape and normalization are taken into account in the analysis using data-driven techniques described in the following sections. The variation of the four-body signal shapes is illustrated with two cases of the mass splitting (10, 30 GeV).

To maintain sensitivity over a large range of Δm values, several signal regions (SR) and corresponding control regions (CR) are defined as listed in Table 1. Since signal leptons have low p_T, we impose an upper limit of $p_T < 30\,\text{GeV}$ in all SR. Because the lepton p_T spectrum of the signal changes rapidly with Δm, the full range of lepton p_T is subdivided into three bins in the calculation of the final results: 5–12, 12–20, and 20–30 GeV, referred to as L, M and H, respectively. In some muon regions, an additional lepton p_T bin 3.5-5 GeV, referred to as VL, is added in order to increase the sensitivity for the very low mass splitting.

The signal regions labelled as SR1 are designed mainly for low values of Δm, where the b jets produced in the $\tilde{t}$ decays rarely pass the selection thresholds. A veto on b-tagged jets strongly reduces the contribution from $\text{t}\bar{\text{t}}$ events. In addition, in parts of SR1 only events with negatively charged leptons ($Q = -1$) are accepted, using the fact that the remaining W+jets background shows significantly more positively than negatively charged leptons while the signal is symmetric in the lepton charge. The acceptance for leptons is reduced to the central region, $|\eta| < 1.5$. Since p_T^{miss} and H_T are correlated in the studied event topologies, a simultaneous se-

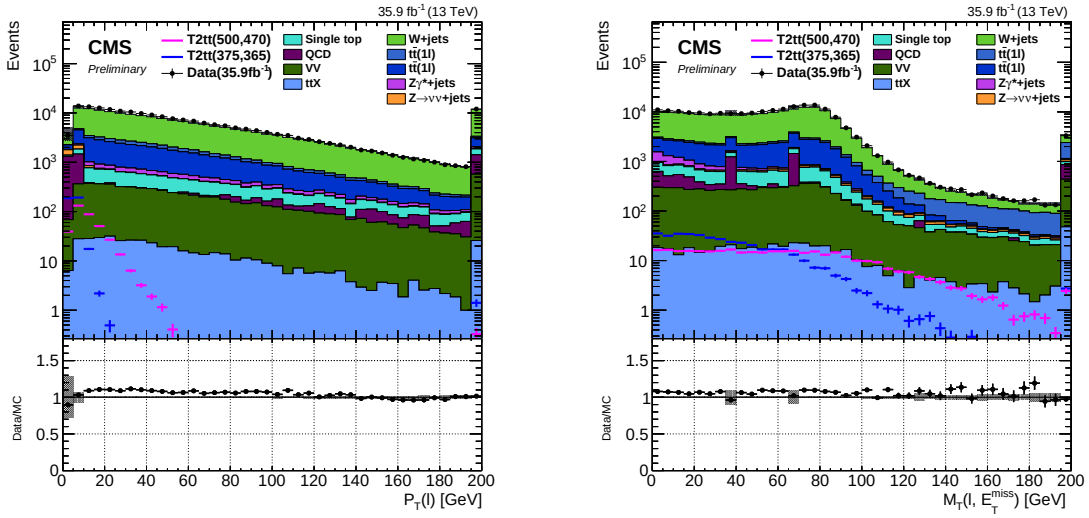

Figure 2: Distributions of (left) lepton p_{T} and (right) m_{T} after the preselection. Data are indicated by dots. The background distributions from simulation are represented as filled, stacked histograms, and the shapes for two example signal points as dashed lines. The error bars and the dark, shaded bands indicate the statistical uncertainties of data and simulation, respectively. The lower panels show the ratio of data to the sum of the SM backgrounds.

lection is applied by using the combined variable $C_{\mathrm{T1}} \equiv \min(p_{\mathrm{T}}^{\mathrm{miss}}, H_{\mathrm{T}} - 100\,\mathrm{GeV})$. The choice of this variable is based on the correlation between $p_{\mathrm{T}}^{\mathrm{miss}}$ and H_{T} in both main backgrounds and signal. An interval in this combined variable carves an L-shaped region in the two-dimensional space of the corresponding two variables. The requirements on $p_{\mathrm{T}}^{\mathrm{miss}}$ and H_{T} from preselection, equivalent to $C_{\mathrm{T1}} > 200\,\mathrm{GeV}$, are tightened to $C_{\mathrm{T1}} > 300\,\mathrm{GeV}$ in SR1.

The second set of signal regions (SR2) mainly targets signals with higher mass splitting, where some of the b jets enter the acceptance. Therefore, the b-jet veto in the region $30 < p_{\mathrm{T}}(\text{b-jet}) < 60\,\mathrm{GeV}$ is reversed, and at least one such jet is required. Events with one or more b-tagged jets with $p_{\mathrm{T}}(\text{b-jet}) > 60\,\mathrm{GeV}$ are still rejected to reduce the $\mathrm{t\bar{t}}$ background. The requirement on C_{T1} used in SR1 is replaced with a requirement on a variable $C_{\mathrm{T2}} \equiv \min(p_{\mathrm{T}}^{\mathrm{miss}}, p_{\mathrm{T}}(\text{leading jet}) - 25\,\mathrm{GeV})$ of $C_{\mathrm{T2}} > 300\,\mathrm{GeV}$ that is more effective in rejecting the remaining $\mathrm{t\bar{t}}$ background enhanced by the reverted soft b-tag condition.

For signal points at low Δm, m_{T} is typically small, mainly due to the soft lepton p_{T} spectrum. With increasing Δm, the average m_{T} increases and eventually the distribution extends to values above $m(\mathrm{W})$. To cover the full range of Δm values, each SR is therefore divided into three subregions, a–c, defined by $m_{\mathrm{T}} < 60\,\mathrm{GeV}$, $60 < m_{\mathrm{T}} < 95\,\mathrm{GeV}$, and $m_{\mathrm{T}} > 95\,\mathrm{GeV}$, respectively. In addition, each subregion in SR1 (SR2) is divided into two by the value of C_{T1} (C_{T2}) of 400 GeV. The letters X and Y are used to refer to the low and high C_{T1} and C_{T2} regions, respectively.

4.1 Background estimation

The following background contributions are estimated by using data: W+jets and $\mathrm{t\bar{t}}$ production with a prompt lepton in the final state, which are the dominant components in most of the signal regions, and backgrounds due to nonprompt leptons from $(\mathrm{Z} \to \nu\nu)$+jets and multijet production, as well as W+jets and $\mathrm{t\bar{t}}$ events with a lost prompt lepton. Rare backgrounds with prompt leptons (other Z/γ^* processes, diboson, single top quark production, and production of $\mathrm{t\bar{t}}$ with an additional W, Z or γ) are predicted from simulation.

The prompt W+jets and $\mathrm{t\bar{t}}$ yields from simulation are normalized in control regions associated

Table 1: Definition of signal regions and their corresponding control regions. The subregions of signal regions are denoted by tags in parentheses described in the text. For jets, the attributes "soft" and "hard" refer to the p_T ranges 30–60 GeV and > 60 GeV, respectively.

Variable	common to all SRs					
Number of hard jets	≤ 2					
$\Delta\phi$(hard jets) (rad)	< 2.5					
p_T^{miss} (GeV)	> 300					
Lepton rejection	no τ, or additional ℓ with $p_T > 20$ GeV					
	SR1			SR2		
H_T (GeV)	> 400			> 300		
p_T(ISR jet) (GeV)	> 100			> 325		
Number of b jets	0			$\geq$1 soft, 0 hard		
$\lvert\eta(\ell)\rvert$	< 1.5			< 2.4		
	SR1a	SR1b	SR1c	SR2a	SR2b	SR2c
m_T (GeV)	< 60	60–95	> 95	< 60	60–95	> 95
$Q(\ell)$	-1	-1	any	any	any	any
$p_T(\mu)$ (GeV)	3.5–5 (VL)	3.5–5 (VL)	-	3.5–5 (VL)	3.5–5 (VL)	-
p_T(e, μ) (GeV)	5–12 (L)	5–12 (L)	5–12 (L)	5–12 (L)	5–12 (L)	5–12 (L)
	12–20 (M)	12–20 (M)	12–20 (M)	12–20 (M)	12–20 (M)	12–20 (M)
	20–30 (H)	20–30 (H)	20–30 (H)	20–30 (H)	20–30 (H)	20–30 (H)
	> 30 (CR)	> 30 (CR)	> 30 (CR)	> 30 (CR)	> 30 (CR)	> 30 (CR)
C_T (GeV)	$300 < C_{T1} < 400$ (X)			$300 < C_{T2} < 400$ (X)		
	$C_{T1} > 400$ (Y)			$C_{T2} > 400$ (Y)		

to each set of signal regions sharing the same selection except the requirement on the lepton p_T. Control and signal regions differ thus only by the lepton p_T range: in the CRs a lepton with $p_T > 30$ GeV is required. The purity of the control regions is typically between 80% and 90%. The simulation is normalized to data after subtracting nonprompt and rare backgrounds from the observed yields in the CR. The obtained scale factors vary from 0.86 to 1.25.

Each factor is applied to all corresponding lepton p_T signal region bins as defined in Table 1. Systematic uncertainties are assigned related to the statistical uncertainties of the factors, and to the shape of the p_T spectrum as described later in this section. The sample composition in the control regions as obtained from simulation is shown in Table 2.

After applying the signal selection, with the exception of the requirement on lepton p_T, the lepton p_T spectra of $t\bar{t}$ and W+jets events are similar. A variation of the $t\bar{t}$ to W+jets cross section ratio of up to 20% is taken into account in the systematic uncertainty.

The extrapolation of the correction factors from control to signal regions has been validated by comparing corrected yields from simulation to data in validation regions. Each of these validation regions is defined by one of the following changes with respect to the signal selection: (a) replacing of the C_{T1} (in SR1) or C_{T2} (in SR2) requirement by $200 < C_T < 300$ GeV, (b) replacing the conditions on b-tagged jets by requiring at least one b-tagged jet with $p_T > 60$ GeV. The predictions in the validation regions are compatible with the observations within uncertainties.

At high values of m_T, namely in the SR1c and SR2c regions, a smaller fraction of W+jets and $t\bar{t}$ events pass the selection criteria. In these regions, especially at low p_T, the contribution of nonprompt background associated to jets but passing impact parameter and isolation requirements becomes comparable to that of prompt backgrounds. This nonprompt background is estimated fully from data in all signal and control regions. For this purpose, an "application region" is assigned to each signal or control region. In this application regions, the isolation and impact

Table 2: Simulated background contributions to control regions normalized to a luminosity of 35.9 fb^{-1}. The nonprompt contributions are estimated from data. Only statistical uncertainties are reported.

Region	W+jets	$\mathrm{t\bar{t}}$	Nonprompt	Rare	Total SM	Data
CR1aX	2133 $\pm$20	226.6$\pm$ 3.5	44.5$\pm$6.4	293.2$\pm$5.9	2698 $\pm$22	2945
CR1aY	878.3 $\pm$8.6	65.8 $\pm$ 1.9	13.3$\pm$3.6	139.4$\pm$4.1	1097 $\pm$10	1197
CR1bX	1107 $\pm$15	134.5$\pm$ 2.7	7.8 $\pm$2.7	112.1$\pm$4.1	1361 $\pm$16	1462
CR1bY	438.2 $\pm$6.4	35.1 $\pm$ 1.4	1.6 $\pm$1.6	51.9 $\pm$2.9	526.8 $\pm$7.3	502
CR1cX	642 $\pm$11	103.8$\pm$ 2.3	12.7$\pm$3.0	174.3$\pm$5.5	932 $\pm$13	1051
CR1cY	278.3 $\pm$8.3	25.5 $\pm$ 1.2	6.2 $\pm$2.2	102.2$\pm$4.3	412.2 $\pm$9.6	432
CR2aX	171.7 $\pm$2.5	195.6$\pm$ 3.3	1.9 $\pm$1.9	64.2 $\pm$1.9	433.4 $\pm$4.9	451
CR2aY	74.54 $\pm$0.98	58.4 $\pm$ 1.7	0.78$\pm$0.78	25.6 $\pm$1.1	159.3 $\pm$2.4	145
CR2bX	104.9 $\pm$2.0	110.8$\pm$ 2.5	1.2 $\pm$1.2	39.2 $\pm$1.6	256.1 $\pm$3.8	226
CR2bY	42.59 $\pm$0.78	30.8 $\pm$ 1.3	0.3 $\pm$0.3	14.96$\pm$0.93	88.6 $\pm$1.8	79
CR2cX	17.26 $\pm$0.79	53.8 $\pm$ 1.7	1.7 $\pm$1.2	15.7 $\pm$1.0	88.4 $\pm$2.4	106
CR2cY	7.50 $\pm$0.84	12.77$\pm$ 0.81	0.6 $\pm$0.6	6.61 $\pm$0.66	27.5 $\pm$1.5	29

parameter conditions are loosened and leptons passing the tight conditions are excluded. The ratio of nonprompt yields in tight and loose regions is measured in dedicated control samples with enhanced QCD multijet background as a function of the lepton p_{T} and $|\eta|$. The systematic uncertainty due to possible different flavor content of jets in the samples used for the measurement of this ratio and in the application regions is assessed by varying the b-tag requirement in the control samples. The effect of this modification varies from 20% to 50% from low to high p_{T}. The nonprompt background estimate in each signal and control region is obtained from the data yield in the corresponding application region, rescaled by the measured ratio, after subtracting the simulated prompt contribution. The consistency of the method is confirmed using simulation. An additional uncertainty of 20% to 200% is assigned in some regions, typically dominated by prompt background, to account for any residual deviation found in this test.

A summary of the expected contributions of different background processes to the signal regions is shown in Table 3 together with the observed data yields.

4.2 Background systematic uncertainties

In addition to the systematic uncertainties described in the previous subsections, various systematic effects and associated uncertainties related to possible shortcomings in the background simulation have been evaluated. Transverse momentum distributions of W bosons and top quarks in respective production processes have been compared to simulation in very pure control samples. Based on these comparisons, the p_{T} spectra in the corresponding background samples were reweighted. To assess the sensitivity of the result to this correction the weights were varied by the size of the correction for W+jets and 50% of the correction for $\mathrm{t\bar{t}}$. An uncertainty of 50% is assigned to the cross sections of all non-leading backgrounds and propagated through the full estimation procedure.

An overview of all systematic uncertainties related to the background prediction is presented in Table 4. The dominant uncertainties are related to the description of the W boson transverse momenta in the W+jets background and to the uncertainties in the jet energy scale.

Table 3: Summary of expected background and observed data yields in the signal regions. The uncertainties on the background prediction include the statistical and systematic sources.

Region	W+jets	$t\bar{t}$	Nonprompt	Rare	Total SM	Data
SR1VLaX	28.8±3.4	2.80±0.55	10.7±4.4	3.4±1.8	45.7±5.9	64
SR1LaX	182±14	22.4±3.6	22.2±8.7	20.1±9.7	247±21	229
SR1MaX	230±18	27.2±4.2	1.7±2.7	29±14	288±26	281
SR1HaX	265±20	30.8±4.8	1.3±2.4	32±15	329±28	351
SR1VLaY	6.44±0.97	0.60±0.21	3.9±2.1	0.85±0.56	11.8±2.4	23
SR1LaY	60.0±5.7	5.4±1.4	6.9±3.4	8.8±4.4	81.2±8.4	68
SR1MaY	73.7±6.7	6.6±1.6	1.4±2.8	9.6±4.7	91.3±9.2	92
SR1HaY	92.9±8.5	7.2±1.7	0.7±1.8	12.5±6.1	113±11	89
SR1VLbX	18.0±2.3	1.48±0.35	17.4±5.9	1.9±1.0	38.8±6.5	48
SR1LbX	118.4±9.1	13.7±2.2	15.2±6.0	10.9±5.6	158±13	152
SR1MbX	133.2±9.7	15.9±2.5	2.1±2.2	14.4±7.3	166±14	163
SR1HbX	148±10	18.9±2.9	0.7±1.1	14.2±6.9	182±14	180
SR1VLbY	4.37±0.80	0.57±0.19	6.1±2.6	0.91±0.61	11.9±2.8	15
SR1LbY	25.9±2.8	1.97±0.53	2.2±1.2	2.6±1.5	32.6±3.6	39
SR1MbY	33.6±3.5	2.26±0.62	0.6±1.2	2.5±1.4	39.0±4.1	39
SR1HbY	41.0±4.0	2.77±0.72	0.25±0.53	4.2±2.2	48.3±4.8	56
SR1LcX	14.0±2.3	2.46±0.59	16.7±3.9	5.2±2.8	38.4±5.5	43
SR1McX	34.8±8.5	6.9±1.4	5.1±1.8	9.6±4.9	56±11	56
SR1HcX	40.5±5.5	10.6±2.2	1.66±0.69	14.1±6.9	67±10	72
SR1LcY	5.8±1.3	0.64±0.25	12.9±3.2	3.7±2.1	23.1±4.1	16
SR1McY	7.5±1.5	1.81±0.63	1.47±0.78	4.5±2.6	15.4±3.3	19
SR1HcY	10.0±1.9	2.67±0.87	0.41±0.27	6.4±3.3	19.5±4.1	29
SR2VLaX	2.74±0.43	2.54±0.50	9.5±3.2	0.64±0.36	15.4±3.3	12
SR2LaX	16.0±1.7	16.7±2.2	5.6±2.0	6.3±3.0	44.6±4.9	39
SR2MaX	21.7±2.3	21.0±2.6	1.57±0.97	9.3±4.4	53.5±6.0	43
SR2HaX	24.6±2.6	22.8±2.9	0.44±0.49	8.7±4.1	56.5±6.2	65
SR2VLaY	0.75±0.17	0.44±0.17	0.96±0.90	0.064±0.041	2.21±0.94	4
SR2LaY	5.09±0.83	4.48±0.98	4.2±1.7	1.98±0.96	15.8±2.5	11
SR2MaY	6.2±1.0	4.64±0.96	0.53±0.53	2.3±1.1	13.7±2.0	16
SR2HaY	6.8±1.1	5.3±1.1	0.50±0.62	2.5±1.2	15.2±2.2	23
SR2VLbX	1.99±0.38	1.03±0.27	2.3±1.4	1.05±0.58	6.3±1.6	3
SR2LbX	11.9±1.7	8.4±1.3	7.0±2.2	5.2±2.5	32.5±4.3	37
SR2MbX	11.7±1.6	8.8±1.4	0.84±0.55	4.5±2.2	26.0±3.5	35
SR2HbX	12.0±1.7	10.5±1.6	0.30±0.38	4.7±2.2	27.6±3.7	36
SR2VLbY	0.55±0.15	0.24±0.10	1.13±0.80	0.36±0.26	2.27±0.87	1
SR2LbY	2.96±0.59	1.63±0.47	0.38±0.41	0.73±0.38	5.7±1.1	6
SR2MbY	3.42±0.68	1.67±0.47	0.36±0.4	1.45±0.73	6.9±1.3	12
SR2HbY	4.05±0.81	2.59±0.68	0.20±0.21	1.15±0.57	8.0±1.4	8
SR2LcX	0.62±0.22	2.1±0.5	3.4±1.7	0.39±0.26	6.5±1.8	6
SR2McX	1.00±0.29	6.4±1.2	2.2±1.3	0.82±0.45	10.5±1.9	11
SR2HcX	1.41±0.43	7.3±1.3	0.23±0.21	1.72±0.99	10.7±1.8	12
SR2LcY	0.36±0.27	0.44±0.21	1.56±0.97	0.22±0.18	2.6±1.1	6
SR2McY	0.207±0.080	0.58±0.25	0.68±0.52	0.17±0.12	1.64±0.62	1
SR2HcY	0.31±0.12	1.42±0.52	0.31±0.24	0.76±0.48	2.81±0.79	3

Table 4: Relative systematic uncertainties in % on the total background prediction in individual signal regions merged in p_T.

Systematic Effect	SR1aX	SR1aY	SR1bX	SR1bY	SR1cX	SR1cY	SR2aX	SR2aY	SR2bX	SR2bY	SR2cX	SR2cY
W+jets-p_T reweighting	4.5	4.8	4.9	4.7	6.2	10.2	2.3	3.7	1.9	1.7	2.2	4.4
$t\bar{t}$-ISR reweighting	0.2	0.1	0.2	0.2	0.4	0.5	<0.1	0.2	0.1	0.1	0.8	0.7
Pileup	0.1	0.2	0.2	0.5	1.8	0.7	0.1	0.2	0.7	0.7	2.0	1.5
b-tag efficiency light jets	<0.1	<0.1	<0.1	<0.1	0.1	0.2	<0.1	0.3	0.1	0.2	0.5	0.9
b-tag efficiency heavy jets	<0.1	0.1	<0.1	0.1	0.1	0.1	0.1	<0.1	<0.1	0.1	0.2	0.4
Jet energy scale	2.1	1.2	1.6	1.6	2.4	1.6	0.9	0.9	1.3	1.4	1.2	0.1
Jet energy resolution	0.3	0.1	0.5	0.3	0.2	0.2	0.1	0.4	0.2	0.2	1.1	0.3

5 Results and interpretation

The observed data and background predictions for all signal regions are summarized in Fig. 3.

The modified-frequentist CL_S criterion [41–43] with a one-sided profile likelihood ratio test statistic is used in the asymptotic formulation [44] to define 95% confidence level (CL) upper limits on the production cross section as a function of the sparticle masses. Statistical uncertainties related to the observed number of events in CRs are modelled as Poisson distributions. All other uncertainties are assumed to be multiplicative and are modelled with log-normal distributions. The impact of a potential signal contamination in the control regions is taken into account by including the control regions, with the estimate of the corresponding signal yield, in the likelihood fit.

Systematic uncertainties in the signal yields related to the determination of the integrated luminosity [45] (2.5%), pileup (1%), renormalization and factorization scales (2-3%), energy scales (up to 4%), object identification efficiencies (up to 5%), and the modelling of ISR (≈6%) have been evaluated. These systematic uncertainties are treated as correlated between signal regions. The statistical uncertainties of the signal simulation typically range between 8%-15%.

The limits obtained for top squark pair production are shown in Figs. 4 and 5, under the assumption of a 100% branching fraction for the four-body decay $\tilde{t} \to bff'\tilde{\chi}_1^0$, and of the chargino-mediated decay $\tilde{t} \to b\tilde{\chi}^+ \to bff'\tilde{\chi}_1^0$, respectively. By using the $\tilde{t}$ pair production cross section calculated at NLO + next-to-leading logarithm (NLL) precision [46–50], the cross section limits can be converted into excluded regions in the $\tilde{t}$–$\tilde{\chi}_1^0$ mass plane. Uncertainties in these cross sections are determined as detailed in Ref. [51].

6 Conclusions

A search for supersymmetry with compressed mass spectra is performed in events with at least one soft lepton, moderate to high values of p_T^{miss}, and one or two hard jets, compatible with the emission of initial-state radiation. The data sample corresponds to 35.9 fb^{-1} of proton-proton collisions recorded by the CMS experiment at $\sqrt{s} = 13$ TeV.

The target of this search is the pair production of top squarks with a mass splitting of at most 80 GeV with respect to the LSP. At small mass splitting, lepton momenta are low, and the b jets do not enter the acceptance. At higher values of Δm, the average lepton momentum increases and soft b jets can be reconstructed. Therefore, signal regions are divided depending on the presence or absence of a soft b-tagged jet and further sub-divided based on the the leading lepton p_T. The transverse mass of the lepton-p_T^{miss} system is used as an additional discriminant.

The main backgrounds to this search are W+jets and $t\bar{t}$ production. Contributions to the sig-

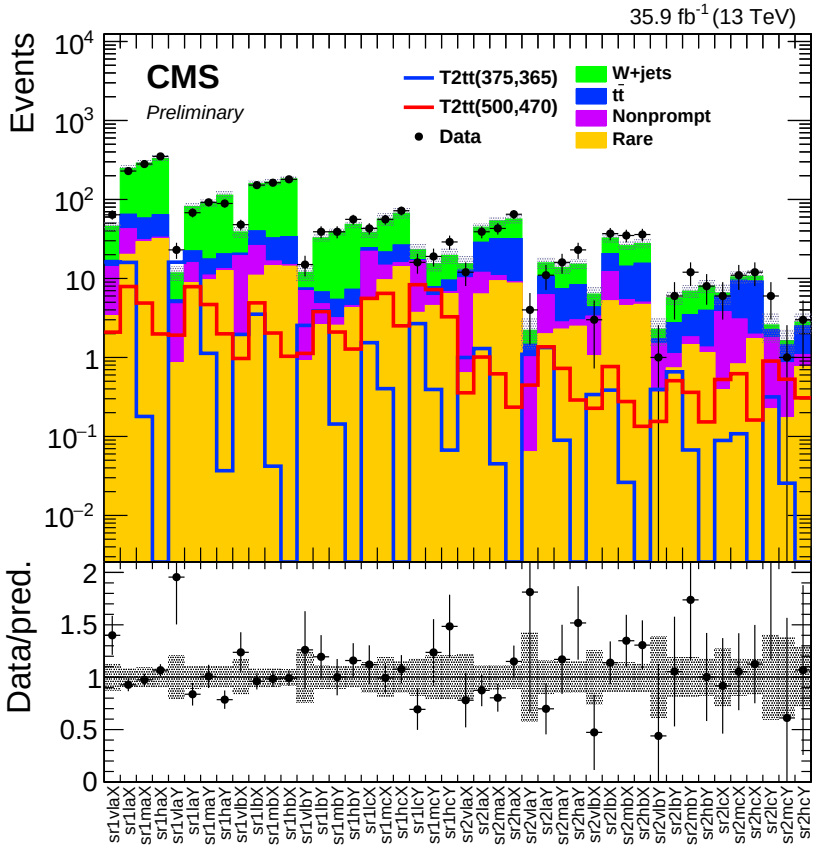

Figure 3: Summary of observed and expected background yields in all signal regions. The vertical bars and the shaded areas represent the statistical uncertainty of the data and the total uncertainty in the prediction, respectively. The lower panel shows the ratio of data to prediction.

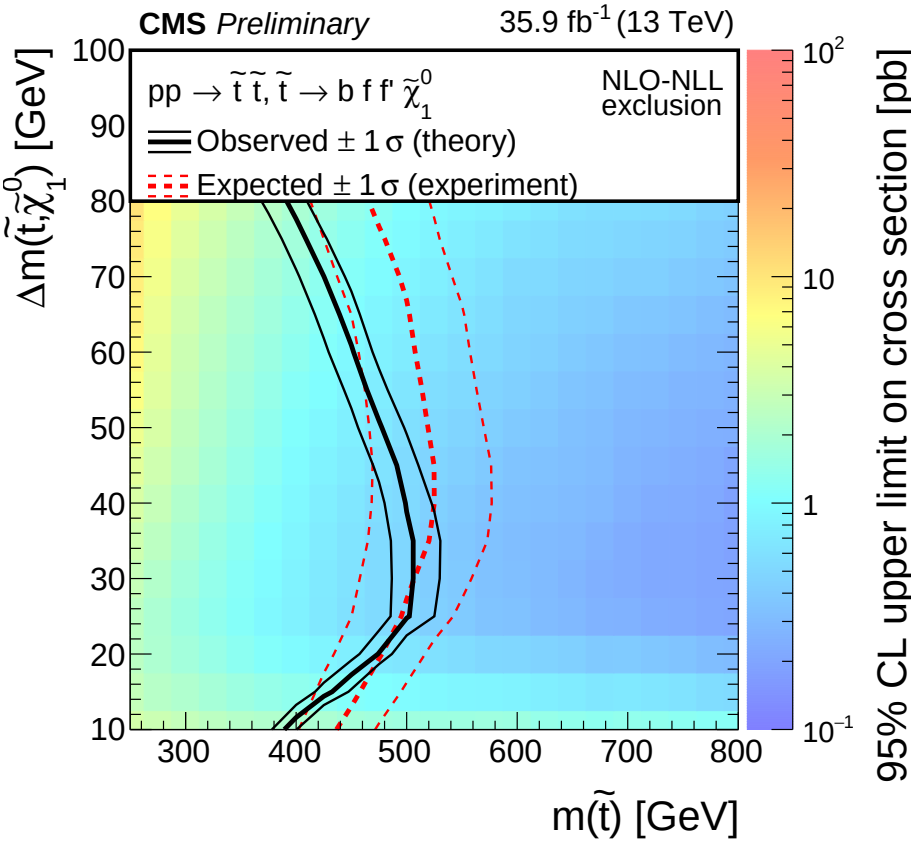

Figure 4: Limits at 95% CL for the four-body decay of the top squark in the $m(\tilde{t})$–$\Delta m(\tilde{t}, \tilde{\chi}_1^0)$ plane. The colour shading corresponds to the observed limit on the cross section. The solid (dashed) lines show the observed (expected) mass limits, derived using the expected top squark pair production cross section. The thick lines representing the central values and the thin lines the variations due to the theoretical (experimental) uncertainties.

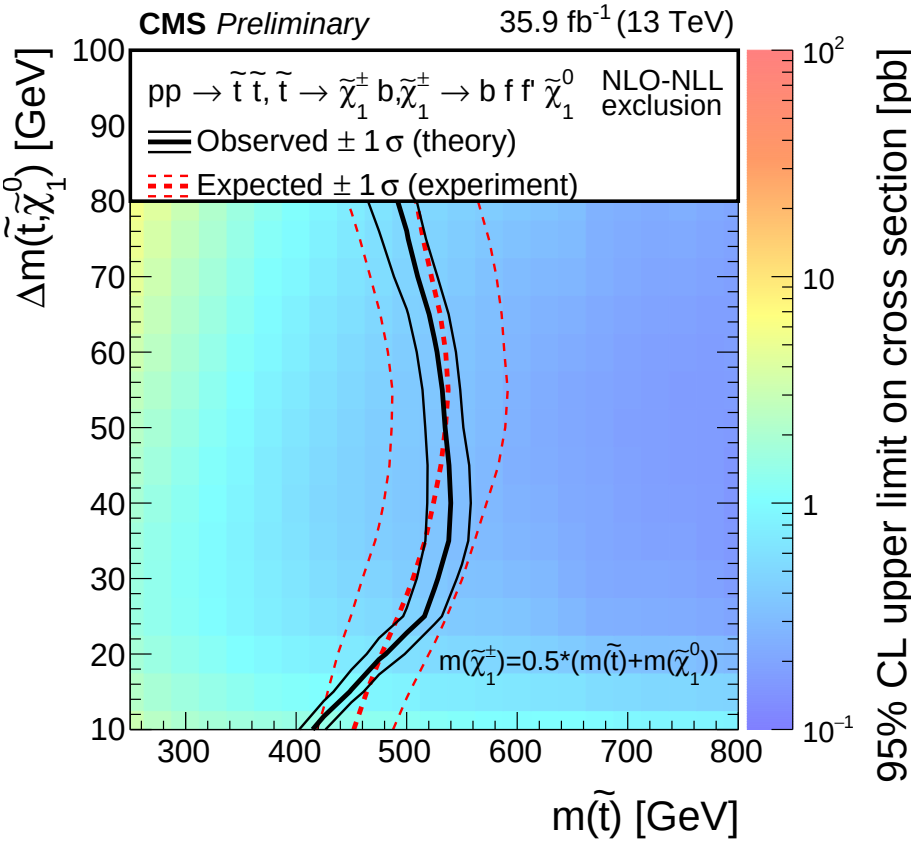

Figure 5: Limits at 95% CL for the chargino-mediated decay of the top squark in the $m(\tilde{t})$–$\Delta m(\tilde{t}, \tilde{\chi}_1^0)$ plane. The colour shading corresponds to the observed limit on the cross section. The solid (dashed) lines show the observed (expected) mass limits, derived using the expected top squark pair production cross section. The thick lines representing the central values and the thin lines the variations due to the theoretical (experimental) uncertainties.

nal regions from these background sources are estimated by using data in control regions to normalize the simulated yields. These estimates are tested with data in validation regions. Background from $(Z \to \nu\nu)$+jets or multijet events with nonprompt lepton passing the analysis selection are estimated fully from data.

The observations in the signal regions are compatible with the SM background predictions. In the absence of any indication of signal, cross section limits are set at 95% CL in the $\widetilde{t}$–$\widetilde{\chi}_1^0$ mass plane. These results are used to extract mass limits based on a reference cross section for top squark pair production and assuming a 100% branching fraction for either the four-body or the chargino-mediated decays of the $\widetilde{t}$. $\widetilde{t}$ masses of up to 500 GeV and 540 GeV are excluded at 95% confidence level for the four-body and the chargino-mediated decays respectivly. The sensitivity of this analysis exceeds that of previous single-lepton searches [16, 52] and is similar to the sensitivity obtained in searches with 2016 data in other final states [18].

References

[1] J. Wess and B. Zumino, "Supergauge transformations in four dimensions", *Nucl. Phys. B* **70** (1974) 39, doi:10.1016/0550-3213(74)90355-1.

[2] R. Barbieri, S. Ferrara, and C. A. Savoy, "Gauge models with spontaneously broken local supersymmetry", *Phys. Lett. B* **119** (1982) 343, doi:10.1016/0370-2693(82)90685-2.

[3] H. P. Nilles, "Supersymmetry, supergravity and particle physics", *Phys. Reports* **110** (1984) 1, doi:10.1016/0370-1573(84)90008-5.

[4] H. E. Haber and G. L. Kane, "The search for supersymmetry: Probing physics beyond the standard model", *Phys. Reports* **117** (1985) 75, doi:10.1016/0370-1573(85)90051-1.

[5] S. Dawson, E. Eichten, and C. Quigg, "Search for supersymmetric particles in hadron-hadron collisions", *Phys. Rev. D* **31** (1985) 1581, doi:10.1103/PhysRevD.31.1581.

[6] E. Witten, "Dynamical breaking of supersymmetry", *Nucl. Phys. B* **188** (1981) 513, doi:10.1016/0550-3213(81)90006-7.

[7] S. Dimopoulos and H. Georgi, "Softly broken supersymmetry and SU(5)", *Nucl. Phys. B* **193** (1981) 150, doi:10.1016/0550-3213(81)90522-8.

[8] G. R. Farrar and P. Fayet, "Phenomenology of the production, decay, and detection of new hadronic states associated with supersymmetry", *Phys. Lett. B* **76** (1978) 575, doi:10.1016/0370-2693(78)90858-4.

[9] R. Barbieri and G. Giudice, "Upper bounds on supersymmetric particle masses", *Nucl. Phys. B* **306** (1988) 63, doi:10.1016/0550-3213(88)90171-X.

[10] B. de Carlos and J. Casas, "One-loop analysis of the electroweak breaking in supersymmetric models and the fine-tuning problem", *Phys. Lett. B* **309** (1993) 320, doi:10.1016/0370-2693(93)90940-J, arXiv:hep-ph/9303291.

[11] M. Dine, W. Fischler, and M. Srednicki, "Supersymmetric technicolor", *Nucl. Phys. B* **189** (1981) 575, doi:10.1016/0550-3213(81)90582-4.

[12] S. Dimopoulos and S. Raby, "Supercolor", *Nucl. Phys. B* **192** (1981) 353, doi:10.1016/0550-3213(81)90430-2.

[13] N. Sakai, "Naturalness in supersymmetric GUTS", *Z. Phys. C* **11** (1981) 153, doi:10.1007/BF01573998.

[14] R. K. Kaul and P. Majumdar, "Cancellation of quadratically divergent mass corrections in globally supersymmetric spontaneously broken gauge theories", *Nucl. Phys. B* **199** (1982) 36, doi:10.1016/0550-3213(82)90565-X.

[15] C. Balázs, M. Carena, and C. E. M. Wagner, "Dark matter, light stops and electroweak baryogenesis", *Phys. Rev. D* **70** (2004) 015007, doi:10.1103/PhysRevD.70.015007, arXiv:hep-ph/0403224.

[16] CMS Collaboration, "Search for supersymmetry in events with at least one soft lepton, low jet multiplicity, and missing transverse momentum in proton-proton collisions at $\sqrt{s} = 13$ TeV", CMS Physics Analysis Summary CMS-PAS-SUS-16-031, CERN, Geneva, 2016.

[17] ATLAS Collaboration, "Search for top squarks in final states with one isolated lepton, jets, and missing transverse momentum using 36.1fb^{-1} of $\sqrt{13}$ TeV pp collision data with the ATLAS detector", ATLAS Conference Report ATLAS-CONF-2017-037, CERN, Geneva, May, 2017.

[18] CMS Collaboration, "Search for direct top squark pair production in the all-hadronic final state in proton-proton collisions at sqrt(s) = 13 TeV", CMS Physics Analysis Summary CMS-PAS-SUS-16-049, CERN, Geneva, 2017.

[19] ATLAS Collaboration, "Search for direct top squark pair production in final states with two leptons in $\sqrt{s} = 13$ TeV pp collisions with the ATLAS detector", ATLAS Conference Report ATLAS-CONF-2017-034, CERN, Geneva, May, 2017.

[20] CMS Collaboration, "The CMS experiment at the CERN LHC", *JINST* **3** (2008) S08004, doi:10.1088/1748-0221/3/08/S08004.

[21] CMS Collaboration, "Particle-flow reconstruction and global event description with the CMS detector", (2017). arXiv:1706.04965. Submitted to *JINST*.

[22] M. Cacciari, G. P. Salam, and G. Soyez, "The anti-k_t jet clustering algorithm", *JHEP* **04** (2008) 063, doi:10.1088/1126-6708/2008/04/063, arXiv:0802.1189.

[23] CMS Collaboration Collaboration, "Jet algorithms performance in 13 TeV data", CMS Physics Analysis Summary CMS-PAS-JME-16-003, CERN, Geneva, 2017.

[24] CMS Collaboration, "Jet energy scale and resolution in the CMS experiment in pp collisions at 8 TeV", *JINST* **12** (2017), no. 02, P02014, doi:10.1088/1748-0221/12/02/P02014, arXiv:1607.03663.

[25] CMS Collaboration Collaboration, "Performance of missing energy reconstruction in 13 TeV pp collision data using the CMS detector", CMS Physics Analysis Summary CMS-PAS-JME-16-004, CERN, Geneva, 2016.

[26] CMS Collaboration, "Identification of b-quark jets with the CMS experiment", *JINST* **8** (2013) P04013, doi:10.1088/1748-0221/8/04/P04013, arXiv:1211.4462.

[27] CMS Collaboration Collaboration, "Identification of b quark jets at the CMS Experiment in the LHC Run 2", CMS Physics Analysis Summary CMS-PAS-BTV-15-001, 2016.

[28] CMS Collaboration, "Reconstruction and identification of τ lepton decays to hadrons and ν_τ at CMS", *JINST* **11** (2016), no. 01, P01019, doi:10.1088/1748-0221/11/01/P01019, arXiv:1510.07488.

[29] CMS Collaboration Collaboration, "Performance of reconstruction and identification of tau leptons in their decays to hadrons and tau neutrino in LHC Run-2", CMS Physics Analysis Summary CMS-PAS-TAU-16-002, CERN, Geneva, 2016.

[30] CMS Collaboration, "Performance of electron reconstruction and selection with the CMS detector in proton-proton collisions at $\sqrt{s} = 8$ TeV", *JINST* **10** (2015) P06005, doi:10.1088/1748-0221/10/06/P06005, arXiv:1502.02701.

[31] CMS Collaboration, "Performance of CMS muon reconstruction in pp collision events at $\sqrt{s} = 7$ TeV", *JINST* **7** (2012) P10002, doi:10.1088/1748-0221/7/10/P10002, arXiv:1206.4071.

[32] J. Alwall et al., "The automated computation of tree-level and next-to-leading order differential cross sections, and their matching to parton shower simulations", *JHEP* **07** (2014) 079, doi:10.1007/JHEP07(2014)079, arXiv:1405.0301.

[33] NNPDF Collaboration, "Parton distributions for the LHC Run II", *JHEP* **04** (2015) 040, doi:10.1007/JHEP04(2015)040, arXiv:1410.8849.

[34] S. Alioli, P. Nason, C. Oleari, and E. Re, "NLO single-top production matched with shower in POWHEG: s- and t-channel contributions", *JHEP* **09** (2009) 111, doi:10.1007/JHEP02(2010)011, 10.1088/1126-6708/2009/09/111, arXiv:0907.4076. [Erratum: JHEP02,011(2010)].

[35] E. Re, "Single-top Wt-channel production matched with parton showers using the POWHEG method", *Eur. Phys. J.* **C71** (2011) 1547, doi:10.1140/epjc/s10052-011-1547-z, arXiv:1009.2450.

[36] T. Sjöstrand, S. Mrenna, and P. Skands, "PYTHIA 6.4 physics and manual", *JHEP* **05** (2006) 026, doi:10.1088/1126-6708/2006/05/026, arXiv:hep-ph/0603175.

[37] T. Sjostrand, S. Mrenna, and P. Z. Skands, "A Brief Introduction to PYTHIA 8.1", *Comput. Phys. Commun.* **178** (2008) 852–867, doi:10.1016/j.cpc.2008.01.036, arXiv:0710.3820.

[38] GEANT4 Collaboration, "GEANT4—a simulation toolkit", *Nucl. Instrum. Meth. A* **506** (2003) 250, doi:10.1016/S0168-9002(03)01368-8.

[39] CMS Collaboration, "The fast simulation of the CMS Detector at LHC", *J. Phys. Conf. Ser.* **331** (2011) 032049, doi:10.1088/1742-6596/331/3/032049.

[40] M. Cacciari, G. P. Salam, and G. Soyez, "FastJet user manual", *Eur. Phys. J. C* **72** (2012) 1896, doi:10.1140/epjc/s10052-012-1896-2, arXiv:1111.6097.

[41] T. Junk, "Confidence level computation for combining searches with small statistics", *Nucl. Instrum. Meth. A* **434** (1999) 435, doi:10.1016/S0168-9002(99)00498-2, arXiv:hep-ex/9902006.

[42] A. L. Read, "Presentation of search results: the CL_s technique", *J. Phys. G* **28** (2002) 2693, doi:10.1088/0954-3899/28/10/313.

[43] ATLAS and CMS Collaborations, LHC Higgs Combination Group, "Procedure for the LHC Higgs boson search combination in Summer 2011", Technical Report ATL-PHYS-PUB/2011-11, CMS NOTE 2011/005, 2011.

[44] G. Cowan, K. Cranmer, E. Gross, and O. Vitells, "Asymptotic formulae for likelihood-based tests of new physics", *Eur. Phys. J. C* **71** (2011) 1554, doi:10.1140/epjc/s10052-011-1554-0, 10.1140/epjc/s10052-013-2501-z, arXiv:1007.1727. [Erratum: *Eur. Phys. J. C* **73** (2013) 2501].

[45] CMS Collaboration Collaboration, "CMS Luminosity Measurements for the 2016 Data Taking Period", CMS Physics Analysis Summary CMS-PAS-LUM-17-001, 2017.

[46] W. Beenakker, R. Höpker, M. Spira, and P. M. Zerwas, "Squark and gluino production at hadron colliders", *Nucl. Phys. B* **492** (1997) 51, doi:10.1016/S0550-3213(97)80027-2, arXiv:hep-ph/9610490.

[47] A. Kulesza and L. Motyka, "Threshold resummation for squark-antisquark and gluino-pair production at the LHC", *Phys. Rev. Lett.* **102** (2009) 111802, doi:10.1103/PhysRevLett.102.111802, arXiv:0807.2405.

[48] A. Kulesza and L. Motyka, "Soft gluon resummation for the production of gluino-gluino and squark-antisquark pairs at the LHC", *Phys. Rev. D* **80** (2009) 095004, doi:10.1103/PhysRevD.80.095004, arXiv:0905.4749.

[49] W. Beenakker et al., "Soft-gluon resummation for squark and gluino hadroproduction", *JHEP* **12** (2009) 041, doi:10.1088/1126-6708/2009/12/041, arXiv:0909.4418.

[50] W. Beenakker et al., "Squark and gluino hadroproduction", *Int. J. Mod. Phys. A* **26** (2011) 2637, doi:10.1142/S0217751X11053560, arXiv:1105.1110.

[51] M. Krämer et al., "Supersymmetry production cross sections in pp collisions at $\sqrt{s} = 7$ TeV", (2012). arXiv:1206.2892.

[52] CMS Collaboration, "Search for supersymmetry in events with soft leptons, low jet multiplicity, and missing transverse energy in proton proton collisions at $\sqrt{s}$=8 TeV", *Phys. Lett.* **B759** (2016) 9–35, doi:10.1016/j.physletb.2016.05.033, arXiv:1512.08002.